Optimal directional volatile transport in retronasal olfaction

Rui Ni (倪睿)[a,b,1], Mark H. Michalski[c], Elliott Brown[c], Ngoc Doan[d], Joseph Zinter[d], Nicholas T. Ouellette[a,e], and Gordon M. Shepherd[f]

[a]Department of Mechanical Engineering and Materials Science, Yale University, New Haven, CT 06520; [b]Department of Mechanical and Nuclear Engineering, Pennsylvania State University, University Park, PA 16802; [c]School of Medicine, Yale University, New Haven, CT 06520; [d]Yale's Center for Engineering Innovation and Design, Yale University, New Haven, CT 06520; [e]Department of Civil and Environmental Engineering, Stanford University, Stanford, CA 94305; and [f]Department of Neuroscience, Yale University School of Medicine, New Haven, CT 06520

The ability of humans to distinguish the delicate differences in food flavors depends mostly on retronasal smell, in which food volatiles entrained into the airway at the back of the oral cavity are transported by exhaled air through the nasal cavity to stimulate the olfactory receptor neurons. Little is known whether food volatiles are preferentially carried by retronasal flow toward the nasal cavity rather than by orthonasal flow into the lung. To study the differences between retronasal and orthonasal flow, we obtained computed tomography (CT) images of the orthonasal airway from a healthy human subject, printed an experimental model using a 3D printer, and analyzed the flow field inside the airway. The results show that, during inhalation, the anatomical structure of the oropharynx creates an air curtain outside a virtual cavity connecting the oropharynx and the back of the mouth, which prevents food volatiles from being transported into the main stream toward the lung. In contrast, during exhalation, the flow preferentially sweeps through this virtual cavity and effectively enhances the entrainment of food volatiles into the main retronasal flow. This asymmetrical transport efficiency is also found to have a nonmonotonic Reynolds number dependence: The asymmetry peaks at a range of an intermediate Reynolds number close to 800, because the air curtain effect during inhalation becomes strongest in this range. This study provides the first experimental evidence, to our knowledge, for adaptations of the geometry of the human oropharynx for efficient transport of food volatiles toward the olfactory receptors in the nasal cavity.

retronasal smell | orthonasal smell | fluid dynamics | particle tracking

The role of olfaction in the sense of smell arises from the biomechanics of the flow of odorized air through the nasal cavity to stimulate olfactory receptor cells there. Interest in the flow biomechanics has been focused entirely on the nasal cavity during orthonasal smell, which arises by sniffing (1–5). However, there is increasing interest in retronasal smell (breathing out while having food or drink in our mouths) (6–9). Much of the perception of the flavor of food or drink is because of the volatiles released from the back of the mouth that are carried by the exhaled air from the oropharynx through the nasopharynx to stimulate the olfactory receptor cells in the nasal cavity (10–12). Although the pathways for retronasal airflow have been mapped in the nasal cavity (13, 14), we test here the hypothesis that the airflow biomechanics of the oropharynx are adapted for efficient delivery of the volatiles underlying smell and flavor.

For orthonasal olfaction, the low concentration of odor molecules in the ambient air requires both a high sensitivity of the olfactory receptor cells and complex turbinate structures to recirculate the air. In addition, one tends to sniff in large volumes of air to increase the total amount of volatiles. In contrast, retronasal olfaction involves a high concentration of volatiles delivered by normal exhalation from the back of the mouth during mastication.

In addition to efficiently delivering food volatiles by retronasal smell, the airway must also minimize inhalation of potentially harmful substances in the ambient air. Most animals have an elaborate system of nasal turbinates that filter, warm, and humidify the inhaled air (15). In humans, this system is reduced but still functional together with the mucus membranes and cilia in the rest of the upper airway. It remains unknown if there are mechanisms to protect the lung in the case of nasal inhalation that might draw volatiles from the back of the mouth into the lung. We, therefore, hypothesized that, if the airflow biomechanics facilitate entry of food volatiles into the exhalation retronasal airstream, there might also be a mechanism for minimizing entry of food volatiles into the inhalation orthonasal airstream. Our study provides evidence for both of these mechanisms. Together, these mechanisms provide a basis in fluid biomechanics for delivering odorant molecules to the dual olfactory system.

Materials and Methods

The specific part of the human airway, from the nostrils to the trachea, that was the focus of our study is shown as a red dashed line in Fig. 1. A full 3D model of this airway was acquired from a normal human subject (a 58-y-old non-Hispanic white female) during breath holds in a normal scanning section. This computed tomography (CT) data were originally obtained in a different study for a different purpose and reused for our experiment. The dataset was processed using the OsiriX software to segment the structures including the finest structures, such as the turbinates, and the virtual cavity that connects the oropharynx and back of the oral cavity.

Because the airway is almost symmetrical between left and right, the model was bisected from the vertical midplane to leave only the left one-half of the airway, including the left nasal cavity, to simplify the experiments. Fig. 2A shows the bisected model, including six distinct parts: (i) nostril (Fig. 2A, i), (ii) nasal cavity (Fig. 2A, ii), (iii) nasopharynx (Fig. 2A, iii), (iv) oropharynx (Fig. 2A, iv), (v) a triangular area defined as the virtual cavity connecting parts iv and vi (Fig. 2A, v), (vi) the back of the oral cavity (Fig. 2A, vi), (vii) laryngopharynx (Fig. 2A, vii), and (viii) trachea (Fig. 2A, viii). This model was then negatively molded to create the airway in the software and later printed

Significance

We have analyzed adaptations of the human airway to enhance transport of food volatiles underlying retronasal smell during expiration as well as limit transport in the opposite orthonasal direction toward the lung during inspiration. We show experimentally using an anatomically based flow dynamic model that the structure of the human airway at the back of the mouth enhances the entrainment of volatiles during expiration and minimizes it during inspiration. Unexpectedly, this effect is largest in a small range of flow rates, which coincides with quiet breathing. Our findings provide insight into the retronasal olfaction process and the adaptation of the shape of the human airway.

Fig. 1. Diagram of the human head. The red dashed line marks the region of the nasal cavity, nasopharynx, oropharynx, and trachea that is the subject of this study. Adapted from ref. 16.

out by a Dimension Elite 3D Printer. The final flow chamber is shown in Fig. 2B. The part of the airway from nasopharynx to trachea is open from the front side and sealed with an acrylic plate, providing a window to visualize the flow. Unlike most previous simulations done in the nasal cavity, our experiment focused on the flow near the small virtual cavity at the back of the mouth, which is the entry point of food volatiles into the main airflow. For simplicity, the entire nasal cavity is hidden beneath the opaque material to retain the correct boundary conditions. Note that the printed flow channel is rigid, although the true human airway is somewhat compliant. However, the pressures applied to the airway walls during slow and shallow breath are expected to be too small to deform the walls to any significant degree. The printed model is, therefore, a good approximation of the real airway without considering vigorous chewing, swallowing, or sneezing that will affect the structure geometry. Changes in overall airflow because of changes in patency of the nasal valve are also assumed to be minimal along with changes caused by compliancy of the pharyngeal walls, which will be minimal during quiet breathing as occurs during retronasal smell.

The whole model was placed vertically on a stand to simulate an upright body position during mastication. The model was connected by two tubes near the nostril and trachea to an external water circulation driven by a pump. Although we used water rather than air as the working fluid for more precise flow visualization, the fluid material parameters (such as density and viscosity) can be scaled out using standard fluid mechanics analysis techniques (17, 18). The water was seeded with fluorescent tracer particles 80 μm in diameter with a density of 1.005 g/cm³ that are small enough to follow the flow faithfully. For the flow rates that we consider here, fluid advection is orders of magnitude more significant than diffusion; thus, although the diffusion constant of the tracer particles is quite different from that of odorant molecules, their transport behavior will be the same. The particles were illuminated by six blue light-emitting diode (LED) lights, and their images were captured by an IDT M5 Camera at a frame rate of 200–300 frame per second (fps), depending on the flow rate. Each experiment lasts for ∼100T to collect sufficient statistics, where T is roughly the average time that it takes for particles to be transported from the back of the nasal cavity to the trachea (a distance close to the size of the model). We focus on steady-state flow without considering the transient flows that occur when switching between inhalation and exhalation. Because the flow in the direction perpendicular to the frontal plane was much weaker than in the other two, imaging and tracking the particles in a 2D plane were sufficient to determine the average flow. The images recorded by the camera were processed to obtain particle positions at each time step, and the positions were linked in time into trajectories using a particle tracking system that we have described in detail elsewhere (19, 20). The time-resolved velocity of each particle was then determined by filtering and differentiating the particle tracks (20, 21).

Results

As children, we learn as the first lesson in table manners to keep the mouth closed while chewing, which not only is more courteous but

also, helps to avoid aspiration of the food residuals. We, therefore, assumed no significant air exchange between the oral cavity and the main airway. Movement of jaws and tongues may potentially induce a small amount of airflow carrying the food volatiles into the airway; however, this airflow should be much smaller than the air exchanged in the main airway, or it would tend to drive large food residuals into the airway and increase the risk of choking. In our study, we assumed that the transport of food volatiles into the airway was purely diffusive, relying entirely on the flow inside the main airway to entrain food volatiles into the main stream.

From slow breathing to vigorous coughing and sneezing, we estimate that Reynolds number Re of the flows in the human respiratory system varies from $O(10)$ to $O(10^4)$ (22). During normal breathing, the Reynolds number of the airflow near the trachea is estimated to be 2,000 (23). However, during mastication, the breathing rate tends to be slower to avoid the aspiration of food, resulting in a smaller Re. To match this physiological range of Re, our experiments were conducted with Re ranging from 80 to 1,500.

Fig. 3 shows a color map of the two in-plane velocity components during inhalation and exhalation at the same applied pressure and similar Reynolds numbers. Mean velocity fields are included in the dataset found at www.mne.psu.edu/Rui_Ni/data/meanuv_example.mat, and full trajectory information will be provided on request. The downward- and upward-pointing black arrows in Fig. 3 indicate the main airflow directions. The red arrows in Fig. 3 show the position and the direction of food volatiles entering the airway from the virtual cavity. Fig. 3 *E–H* shows enlarged pictures of the area including the oropharynx (Fig. 2A, *iv*) and the virtual cavity (Fig. 2A, *v*) near the entry point of the food volatiles. As shown in Fig. 3 *A* and *E*, these two parts can be easily distinguished in the flow maps by their vertical velocity during inhalation: in the virtual cavity, the vertical velocity is nearly zero, whereas in the oropharynx, the vertical velocity is large and negative. Simultaneously, the horizontal velocity component in the
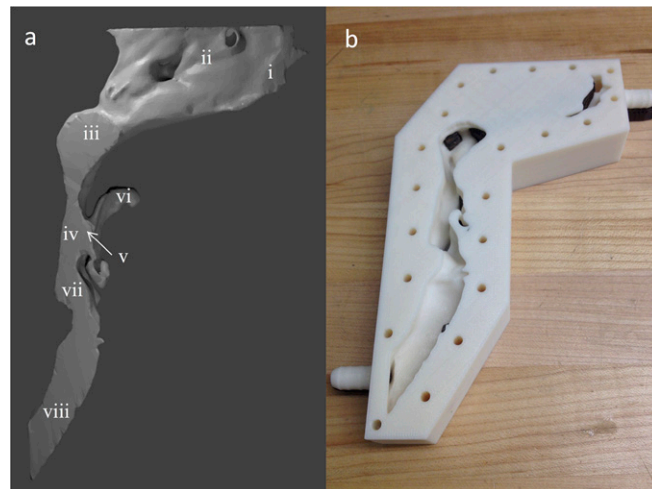
Fig. 2. (A) The bisected 3D model of human airway: (A, *i*) nostril, (A, *ii*) nasal cavity, (A, *iii*) nasopharynx, (A, *iv*) oropharynx, (A, *v*) a triangular area defined as the virtual cavity connecting parts *iv* and *vi*, (A, *vi*) the back of the oral cavity, (A, *vii*) laryngopharynx, and (A, *viii*) trachea. (B) The 3D-printed negative mold of the model is shown in A. Parts in A, *iii*–A, *viii* are opened from the front side, whereas parts in A, *i* and A, *ii* are covered by opaque materials to create the correct boundary conditions. A transparent Plexiglas sheet was used to cover the front side of the model, so that the flow in A, *iii*–A, *viii* could be visualized and measured. Two connectors near A, *i* and A, *viii* are used to link the circulating flow to our model.
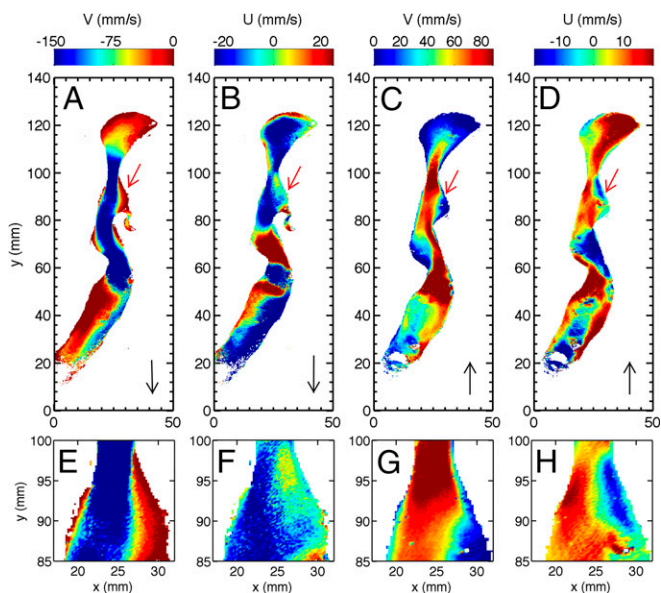
Fig. 3. Two velocity components for experiments with the two different flow directions. (*A*) Vertical velocity *V* in orthonasal flow with Re = 1,008. (*B*) Horizontal velocity *U* in orthonasal flow. (*C* and *D*) Vertical V and horizontal U in retronasal olfaction with Re = 883. (*E*–*H*) Enlarged views close to the virtual cavity opening connected to the back of the mouth. The original data for these two velocity fields are provided in the dataset found at www. mne.psu.edu/Rui_Ni/data/meanuv_example.mat.

virtual cavity, shown in Fig. 3 *B* and *F*, is also close to zero and slightly positive (yellow). These velocity components indicate that the flow in this area is almost stagnant, and it may even gently push food volatiles back into the mouth and prevent them from entering the main airflow. The main flow in the oropharynx functions as an air curtain, preventing food volatiles from being entrained into the main stream, and may help to reduce the risk of aspiration of food into the lower respiratory system.

The flow during exhalation is completely different. Fig. 3 *C*, *D*, *G*, and *H* shows that the flow in the virtual cavity is now not zero; instead, there is a large vertical velocity in the upper right corner of the image that helps to move the food volatiles from the opening of the oral cavity into the main airflow. In the same area, there is a large blue spot in the horizontal component, indicating a large negative horizontal velocity that entrains the food volatiles, moves it leftward to meet the main stream, and carries it upward to the olfactory receptor neurons in the nasal cavity (Fig. 3 *C*, *D*, *G*, and *H*). These measurements qualitatively suggest that, when the airway and the Reynolds number are identical in ortho- and retronasal breathing, the complex anatomical geometry of the airway can create an asymmetric flow that preferentially drives the transport of food volatiles to the nasal cavity during retronasal breathing.

In addition to the average velocity field, our particle tracking technique enabled us to study the transport of individual tracer particles. The white rectangular box shown in Fig. 4*A* in the connection cavity indicates the entry point of food volatiles. By looking only at tracer particles with initial positions inside this box, we characterized their transport by the flow. Fig. 4*A* shows 25 randomly chosen particle trajectories from the same time window in both flow directions at Reynolds numbers close to 900. After being released from the area, the particles, on average, were transported in the mean flow direction as shown. However, during inhalation (red trajectories in Fig. 4*A*), tracers were trapped in the virtual cavity, and as a result, their overall displacement was much smaller than those transported during exhalation. This trapping mechanism during inhalation prevents food volatiles from being transported deeper into the respiratory system. However, depending on the flow

conditions and Re, the fluctuations of the flow will occasionally drive the tracers out of the cavity farther down to the trachea.

To characterize the differences in volatile transport efficiency during inhalation and exhalation statistically, the mean vertical displacement *d* is plotted against the time *t* in Fig. 4*B*; *d* is defined as the relative vertical displacement of an individual tracer after it is released from the virtual cavity and thus, goes to zero at the initial time. The two axes are normalized by the full channel height *L* and a time scale *T*. *T* is determined as $L/\overline{V}$, where $\overline{V}$ is the mean vertical velocity averaged over time and space, including the stagnant areas. Two black dashed lines in Fig. 4*B* extending from origin to (1, 1) and (1, −1) indicate the mean velocity $\overline{V}$ in two directions. Although the net transport in both flow directions was slower than the mean flow, transport during exhalation seemed to reach much farther than during inhalation, giving clear evidence for transport asymmetry. In addition, the curves for exhalation are very close to each other at all three Reynolds number studied. In contrast, there was more variation of the displacement with Reynolds numbers during inhalation. The line closest to zero is the intermediate Reynolds number (around 1,000), which suggests that the Re dependence during inhalation may not be monotonic.

To examine the Reynolds number dependence of the transport asymmetry, Fig. 5*A* shows the normalized mean vertical displacement of tracer particles 0.2*T* after being released from the virtual cavity at different Re. This timespan is chosen to capture the full trajectory of the fastest particles before they leave the finite view area. The sign of the displacement indicates the direction: negative and positive indicate the flow directions during inhalation and exhalation, respectively, whereas the black dashed line in Fig. 5*A* indicates zero displacement. It is apparent that the transport efficiency of food volatiles during exhalation was greater than during inhalation over an equivalent timespan at all measured Reynolds numbers.

Our findings imply that the structure of the airway, especially the part close to the virtual cavity, produces a simple but effective mechanism to ensure the directional transport of food volatiles. In
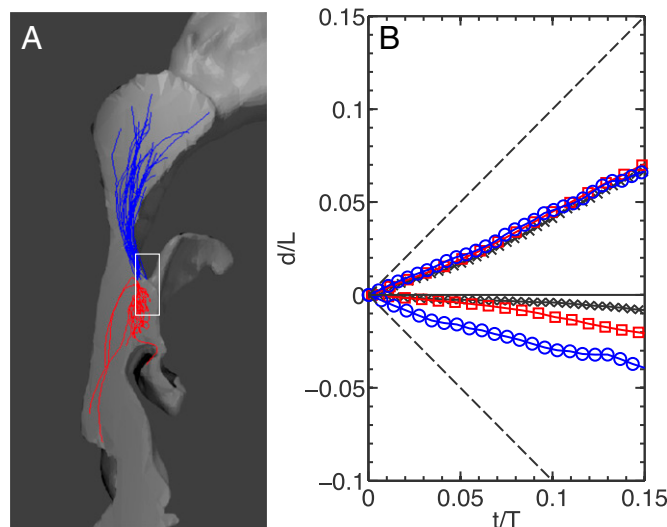
Fig. 4. (*A*) Trajectories of tracer particles with initial positions that are inside the white box. Blue and red trajectories are for exhalation (Re = 883) and inhalation (Re = 1,008), respectively. (*B*) The normalized mean vertical displacement *d* of all trajectories starting from the white box vs. the normalized time. Black crosses, Re = 1,093 (inhalation) and Re = 1,020 (exhalation); blue circles, Re = 131 (inhalation) and Re = 161 (exhalation); red squares, Re = 1,347 (inhalation) and Re = 1,454 (exhalation). Dashed lines represent the case if the particles move with mean vertical velocity $\overline{V}$.
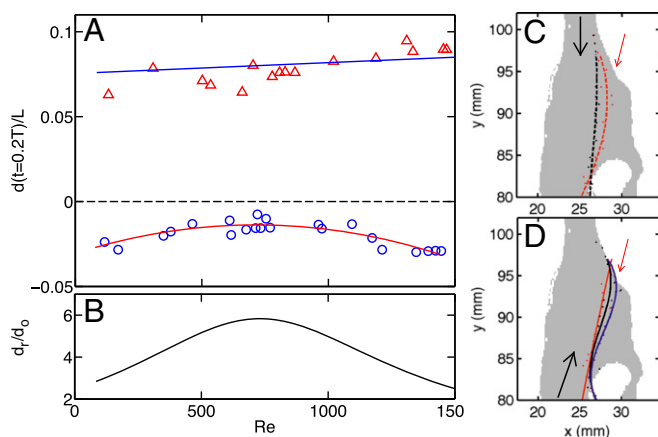
Fig. 5. (A) The mean displacement of tracer particles time $t = 0.2T$ after being released from the virtual connection cavity at different Reynolds numbers. The triangles and circles represent the flow directions during exhalation and inhalation, respectively, and the two groups of symbols are fitted with first and second polynomial functions, respectively. The function forms are shown with two solid lines. (B) The ratio of the two polynomial functions from A to illustrate the ratio between the displacement of tracer transport during exhalation (d_r) and inhalation (d_o). (C) The dividing streamlines inside the virtual connection cavity are shown during orthonasal olfaction at Re = 78 (red) and Re = 1,093 (black). (D) The dividing streamlines are shown at Re = 131 (red), 1,188 (black), and 1,310 (blue). The black arrows indicate the main flow direction. The red arrows represent the position and direction of the entry of the food volatiles into the airway.

addition to the magnitude differences, the Reynolds number dependence for the two directions is quite different: there is a weak but slightly increasing trend for flow during exhalation, but for inhalation, the displacement seems to have a peak at Reynolds numbers of 700–1,000. The peak (meaning the smallest displacement) indicates that, during inhalation, the entrainment of food volatiles from the back of the oral cavity is almost completely inhibited at this Reynolds number and that the air curtain effect performs the best. The Re dependences of the two flow directions can be fitted with first- and second-order polynomial functions as shown by the two solid lines in Fig. 5A. The optimal situation for volatile transport is to maximize the particle displacement during exhalation (denoted d_r) while minimizing it during inhalation (denoted d_o). To quantify this asymmetry in volatile transport, Fig. 5B shows the ratio between d_r and d_o using the two fitted curves. The shape of the d_r/d_o curve resembles that of d_o, because the trend of d_o is much stronger than that of d_r. This result suggests that there is an optimal Reynolds number at which the transport asymmetry is maximized.

As we discussed earlier for Fig. 3, a qualitative explanation of the asymmetrical transport of food volatile is that, during exhalation, the main flow pushes into the virtual cavity and directly sweeps food volatiles out. To connect this qualitative explanation with the Reynolds number dependence of the displacement, the contours of the vertical velocity at level $\overline{V}$ for different Reynolds numbers are shown in Fig. 5 C (inhalation) and D (exhalation). The small dots represent the contour position, and the lines with the same color indicate a third-order polynomial fit to the symbols (Fig. 5 C and D). Each line separates the high vertical velocity region on the left from the small nearly stagnant area on the right. Because the vertical velocity dominates, these contours should be equivalent to the dividing streamlines that separate the main flow from the small recirculation flow in the virtual cavity. For inhalation (Fig. 5C), the inflow direction is indicated by the black arrow, which points almost straight downward. For very small Reynolds numbers, as shown by the red curve in Fig. 5C, the flow is still able to reattach to the boundary layer near the entry point of the food volatiles and

therefore, increases the chance of carrying the volatiles with it, rendering a relatively large volatile transport efficiency.

With increasing Re, the inflow speed becomes faster, and this dividing streamline starts to detach from the boundary, leading to a large separated flow near the volatile entrance and reducing the entrainment and transport of the volatiles. However, with even higher Re, the flow starts to move from a purely laminar flow state to a transitional flow, meaning that the flow starts to become unstable and the fluctuations of horizontal velocity increase, leading to a new mechanism for drawing volatiles into the airway. When this happens, the contour becomes very unstable and therefore, cannot be uniquely drawn. It is known that the lower end of the transitional Reynolds number range decreases from about 4,000 to about 1,200 when the flow channel changes from a smooth pipe to a backward-facing step; in general, the transitional Reynolds number decreases as the structure of the flow channel becomes more complicated, because more complex boundaries tend to drive fluctuations. Therefore, it is not surprising that the Reynolds number at which we observe strong fluctuations is slightly smaller than 1,200.

During exhalation, the inflow direction, as shown by the black arrows in Fig. 5, is tilted toward the connection cavity. The inertia of the flow, even for this small Reynolds number, is sufficient to reattach the stream to the boundary near the entry point of the volatiles and carry the volatiles with the flow. It is interesting to note that the reattachment position of the flow is very close to the entry point of the food volatiles, which helps to maximize the entrainment efficiency. The higher the Reynolds number, the stronger the inertial effect of the flow and therefore, the deeper the flow can bend into the virtual cavity. However, for the same Reynolds number (close to 1,400), the flow does not enter the transitional regime, in part because the width of the upstream section of the airway during exhalation (the trachea) is much larger than that during inhalation (the nasal cavity). Thus, the inertia of the flow during exhalation acts mainly to force the flow deeper into the virtual cavity rather than destabilizing it. The reason that we did not see a strong increase of the volatile transport efficiency with Reynolds number may be because as long as the main flow can reattach to the boundary near the entry, the entrainment and transport efficiency will change relatively little.

Discussion

An important development in sensory neuroscience is the realization that the sense of smell is really two systems: orthonasal for breathing in and retronasal for breathing out. Paul Rozin (24) was the first to emphasize the "dual sense of smell" (24). Orthonasal smell is used to sense smells in the ambient air, and retronasal smell is used to sense the volatiles released from the back of the mouth during eating and drinking. Many experiments have provided evidence for the neural mechanisms involved in orthonasal smell, and there is increasing evidence for how retronasal smell is combined with the other senses stimulated by food and drink in the mouth to give the perception of flavor (9, 12, 25). Although there have been numerous studies of the biomechanics of orthonasal airflow in the nasal cavity, this is the first study, to our knowledge, of the airflow biomechanics relevant to orthonasal and retronasal smell in the crucial region of the oropharynx, where volatiles from the back of the mouth access the two directions of airflow.

The main results of this study have shown that the structure and function of the oropharynx combine to produce two oppositely directed valve-like actions. With retronasal smell, they create a virtual connection cavity that facilitates the entry of volatiles from the back of the mouth into the exhalation airflow and minimizes entry into the trachea and lungs. With orthonasal smell, an opposite action occurs, in which the incoming airflow creates a virtual curtain that tends to isolate the back of the mouth and inhibit the entry of volatiles into the airstream entering the trachea and lungs.

From an engineering simplism point of view, a proposed minimal set of key features of the structure design can be extracted from our subject. Based on our experimental results, we believe that there are at least three important structures: (*i*) a virtual cavity with the volatile entry near the upside of the cavity, (*ii*) a narrow channel connecting the nasopharynx and oropharynx to enforce the air curtain effect, and (*iii*) a backward-tilted laryngopharynx, which helps to create an inflow sweeping into the virtual cavity. The exact position of the optimal Reynolds number and the ratio of the transport efficiency in different flow directions may depend on many other factors, but these three ingredients could be sufficient to ensure the directional volatile transport, and they will be tested in the future in different human subjects to examine if these structures are universal across different ages, races, and genders.

In summary, the design of the human upper airway appears to have been optimized during evolution to achieve multiple functions, including enhancing the ability of food volatiles from the back of the oral cavity to be transported to the olfactory receptor cells in the nasal cavity. In this paper, we study this problem from an engineering point of view to understand the simple but effective mechanism that nature used. We show that the structure of the airway is able to create asymmetrical transport of food volatiles in different flow directions that is also optimized through a range of intermediate Reynolds numbers. Our results explain why we do not breath rapidly to enhance retronasal smell, because the low flow rate is already suffcient for the efficient transport of the volatiles.

1. Yang GC, Scherer PW, Mozell MM (2007) Modeling inspiratory and expiratory steady-state velocity fields in the Sprague-Dawley rat nasal cavity. *Chem Senses* 32(3): 215–223.
2. Craven BA, Paterson EG, Settles GS, Lawson MJ (2009) Development and verification of a high-fidelity computational fluid dynamics model of canine nasal airflow. *J Biomech Eng* 131(9):091002.
3. Lawson MJ, Craven BA, Paterson EG, Settles GS (2012) A computational study of odorant transport and deposition in the canine nasal cavity: Implications for olfaction. *Chem Senses* 37(6):553–566.
4. Zhao K, Jiang J (2014) What is normal nasal airflow? A computational study of 22 healthy adults. *Int Forum Allergy Rhinol* 4(6):435–446.
5. Lu J, Han D, Zhang L (2014) Accuracy evaluation of a numerical simulation model of nasal airflow. *Acta Otolaryngol* 134(5):513–519.
6. Sun BC, Halpern BP (2005) Identification of air phase retronasal and orthonasal odorant pairs. *Chem Senses* 30(8):693–706.
7. Zhao K, Scherer PW, Hajiloo SA, Dalton P (2004) Effect of anatomy on human nasal air flow and odorant transport patterns: Implications for olfaction. *Chem Senses* 29(5): 365–379.
8. Bojanowski V, Hummel T (2012) Retronasal perception of odors. *Physiol Behav* 107(4): 484–487.
9. Shepherd GM (2012) *Neurogastronomy. How the Brain Creates Flavor and Why It Matters* (Columbia Univ Press, New York).
10. de Araujo IE, Rolls ET, Kringelbach ML, McGlone F, Phillips N (2003) Taste-olfactory convergence, and the representation of the pleasantness of flavour, in the human brain. *Eur J Neurosci* 18(7):2059–2068.
11. Bender G, Hummel T, Negoias S, Small DM (2009) Separate signals for orthonasal vs. retronasal perception of food but not nonfood odors. *Behav Neurosci* 123(3): 481–489.
12. Small DM (2012) Flavor is in the brain. *Physiol Behav* 107(4):540–552.
13. Ishikawa S, Nakayama T, Watanabe M, Matsuzawa T (2006) Visualization of flow resistance in physiological nasal respiration: Analysis of velocity and vorticities using numerical simulation. *Arch Otolaryngol Head Neck Surg* 132(11):1203–1209.
14. Deibler KD (2001) Measuring the effect of food composition on flavor release using the retronasal aroma simulator and solid phase microextraction. PhD thesis (Cornell University, Ithaca, NY).
15. Negus VE (1958) *Comparative Anatomy and Physiology of the Nose and Paranasal Sinuses* (Livingstone, Edinburgh).
16. Shepherd GM (2015) Neuroenology. How the brain creates the taste of wine. *Flavour* 4:19.
17. Munson BR, Rothmayer AP, Okiishi TH (2012) *Fundamentals of Fluid Mechanics* (Wiley, New York).
18. Cengel Y, Cimbala J (2013) *Fluid Mechanics Fundamentals and Applications* (McGraw-Hill Higher Education, New York).
19. Ouellette NT, Xu H, Bodenschatz E (2006) A quantitative study of three-dimensional Lagrangian particle tracking algorithms. *Exp Fluids* 40(2):301–313.
20. Ouellette NT, Xu H, Bodenschatz E (2007) Measuring Lagrangian statistics in intense turbulence. *Springer Handbook of Experimental Fluid Dynamics*, eds Tropea C, Yarin AL, Foss JF (Springer, Berlin), pp 789–799.
21. Mordant N, Crawford AM, Bodenschatz E (2004) Experimental Lagrangian probability density function measurement. *Physica D* 193(1):245–251.
22. Bourouiba L, Dehandschoewercker E, Bush JWM (2014) Violent expiratory events: On coughing and sneezing. *J Fluid Mech* 745:537–563.
23. Horsfield K, Dart G, Olson DE, Filley GF, Cumming G (1971) Models of the human bronchial tree. *J Appl Physiol* 31(2):207–217.
24. Rozin P (1982) "Taste-smell confusions" and the duality of the olfactory sense. *Percept Psychophys* 31(4):397–401.
25. Rolls ET (2015) Taste, olfactory, and food reward value processing in the brain. *Prog Neurobiol* 127-128(2015):64–90.